Free surface flows simulations in Pelton turbines using an hybrid SPH-ALE method

— Source link ☑

Jean-Christophe Marongiu, Francis Leboeuf, Joëlle Caro, Etienne Parkinson

Institutions: École centrale de Lyon

Related papers:

- Simulating Free Surface Flows with SPH

- On particle weighted methods and smooth particle hydrodynamics

- Smoothed particle hydrodynamics

- Numerical simulation of interfacial flows by smoothed particle hydrodynamics

- Smoothed particle hydrodynamics: Theory and application to non-spherical stars

Free surface flows simulations in Pelton turbines using an hybrid SPH-ALE method

Jean-Christophe Marongiu, Francis Leboeuf, Joëlle Caro, Etienne Parkinson

Free surface flows simulations in Pelton turbines using an hybrid SPH-ALE method

Simulation des écoulements à surface libre dans les turbines Pelton par une méthode hybride SPH-ALE

JEAN-CHRISTOPHE MARONGIU, *Laboratory of Fluid Mechanics and Acoustics, UMR CNRS 5509, Ecole Centrale de Lyon, University of Lyon, Ecully, France. E-mail: jc.marongiu@gmail.com (author for correspondence)*

FRANCIS LEBOEUF, *Laboratory of Fluid Mechanics and Acoustics, UMR CNRS 5509, Ecole Centrale de Lyon, University of Lyon, Ecully, France. E-mail: francis.leboeuf@ec-lyon.*

JOËLLE CARO, *Laboratory of Fluid Mechanics and Acoustics, UMR CNRS 5509, Ecole Centrale de Lyon, University of Lyon, Ecully, France. E-mail: joelle.caro@ec-lyon.fr*

ETIENNE PARKINSON, *Hydraulic Research Department, Andritz Hydro, Vevey, Switzerland. E-mail: etienne.parkinson@andritz.com*

ABSTRACT
An Arbitrary Lagrange Euler (ALE) description of fluid flows is used together with the meshless numerical method Smoothed Particle Hydrodynamics (SPH) to simulate free surface flows. The ALE description leads to an hybrid method that can be closely connected to the finite volume approach. It is then possible to adapt some common techniques like upwind schemes and preconditioning to remedy some of the well known drawbacks of SPH like stability and accuracy. An efficient boundary treatment based on a proper upwinding of fluid information at the boundary surface is settled. The resulting SPH-ALE numerical method is applied to simulate free surface flows encountered in Pelton turbines.

RÉSUMÉ
La méthode numérique sans maillage Smoothed Particle Hydrodynamics (SPH) est modifiée par l'adoption d'une description Arbitrary Lagrange Euler (ALE) des écoulements fluides, dans le but de simuler des écoulements à surface libre. Le formalisme ALE conduit à une méthode numérique hybride s'apparentant sur de nombreux points à une approche volumes finis. Il est alors possible d'adapter des techniques numériques courantes comme les schémas décentrés et le préconditionnement pour résoudre certains défauts majeurs de la méthode SPH, comme la stabilité numérique ou le manque de précision. Par ailleurs, le traitement des conditions limites est réalisé par un décentrement approprié des informations fluides sur les surfaces frontières. La méthode numérique SPH-ALE résultante est appliquée à la simulation d'écoulements à surface libre tels que ceux rencontrés dans les turbines Pelton.

Keywords: Hyperbolic equations, Pelton turbine, preconditioning, Riemann problem, SPH-ALE, upwind scheme, water impacts

1 Introduction

1.1 *Description of a Pelton turbine*

The Pelton turbine is a hydraulic impulse machine patented in 1889 by Lester Allan Pelton. This turbine is adapted for high head, from 200 to around 2,000 meters, and low discharge installations, from 5 to $50 \, \mathrm{m^3 \cdot s^{-1}}$. For example, the largest unit worldwide of BIEUDRON in Switzerland can produce a power of 420 MW for a head of more than 1,800 meters. The Pelton turbine is composed of several hydraulic components, see Fig. 1.

The penstock consists in a long pipe coming from the upper dam. It is followed eventually by the "Unit" distributor to distribute the flow between different units of the power plant. The turbine distributor is composed of bends and bifurcations.

Its function is to share evenly the flow between the nozzles (from 1 to 6) from which the jets are ejected towards the runner.

The runner is composed of 18 to 26 buckets usually. Buckets are impacted by the jets. Their role is to transform the kinetic energy of the jet(s) into mechanical energy and finally electric power, the runner shaft being combined with a generator. Design of the buckets is a key issue for the turbine efficiency.

The casing, in which the runner and nozzle(s) are encapsulated, manages the evacuation of the water from the runner and is designed to prevent any disturbance of the flow in the runner and of the jet(s).

In contrast with most of hydraulic turbines, the flow in a Pelton turbine is confined in the penstock, distributor and nozzles and is a free surface flow as soon as it leaves the nozzle.
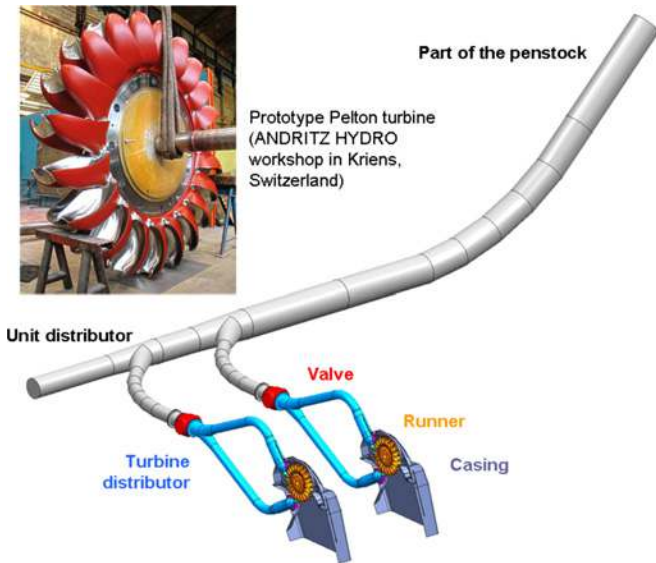
Figure 1 Typical layout of 2 units of 2-jet Pelton turbine (penstock, "unit" distributor, turbine distributor, runner and casing)

1.2 *Value of CFD for Pelton turbine analysis*

Computational Fluid Dynamics (CFD) methods are an opportunity to improve the understanding of the phenomena occurring along the hydraulic parts of the pelton turbine. Indeed, experimental visualisations are difficult in most of the parts of the Pelton turbine and local data flow are very complex to obtain by experiments (see Fig. 2). On the contrary, CFD enables to access to local flow features, and thus to explain flow phenomena and their potential influence on the turbine performances.

This deeper understanding of flows' behaviour makes possible to modify the design of the different components of the turbine and to quantify with CFD analysis the impact of the design modifications on performances. Moreover, as there is an important market for hydraulic power plants refurbishment, CFD analysis eases the diagnosis of the potentials of existing hydraulic Pelton turbine components and to propose better hydraulic solutions, taking into account old fixed components (Parkinson *et al.* 2004), as distributors and casings are often concrete-embedded in large units.

Figure 2 Experimental visualisation of the flow in the casing of a 2-jet Pelton model turbine, Hydraulic laboratory of Andritz Hydro, Switzerland

1.3 *Specificities of Pelton hydraulics*

Flows in Pelton turbines involve various phenomena. In the distributor, one deals with internal flows mainly driven by viscous effects. A careful description of boundary layers and of turbulence are required in order to properly catch flow patterns. Time fluctuations are at the scale of turbulent fluctuations, and so flow can be considered as stationnary and modeled through a time-averaged formalism (so-called *Reynolds Averaged Navier Stokes* equations). From the nozzle(s), flows become free surface flows, involving high speed jets, water sheets, and droplets of various sizes. These flows are mainly governed by inertial and gravitational forces. Because of the presence of a rotor and of a stator, flows can no more be considered as stationnary and time dependence has to be explicitly taken into account. The length/velocity/time scales and physics involved in these different regions are not of the same order in all parts of the turbine, as shown in Table 1. This has a direct consequence on the numerical simulation of these flows, and different approaches adapted to each region must be considered.

Internal flows in the distributor are typicaly simulated using *Finite Volume* (FV) methods. For free surface flows, the *Volume Of Fluids* (VOF) formalism has proved its applicability for Pelton turbines (Kvicinsky *et al.* 2002, Perrig *et al.* 2006). Using this method, care must be brought to the design of the computational mesh in order to improve the description of the free surface, particularly at the rotor/stator interface. Even though, it is hard to remove the numerical diffusion of the free surface, not only at the rotor/stator interface but also when water sheets travel a long distance freely in the air domain.

Simulations of jet(s) impinging a rotating runner are now achieved in the design process (see Fig. 3), but the full simulation of the turbine, including distributor and casing, remains a true challenge involving at least 40 millions of cells (see Fig. 4 and Favre *et al.* 2005). Besides, stability of such a simulation is delicate because of the small spacing between static and rotating parts, which is a difficult point for the rotor/stator mesh interface.

1.4 *Introducing SPH into CFD for Pelton turbines*

Limitations presented above explain why it is difficult to envisage the study of water sheets and their impact on the casing with eulerian (also called mesh-based) numerical methods. At first sight, lagrangian techniques conceptually represent an alternative

Table 1 Typical length and velocity scales in a Pelton turbine at model scale (Perrig 2007)

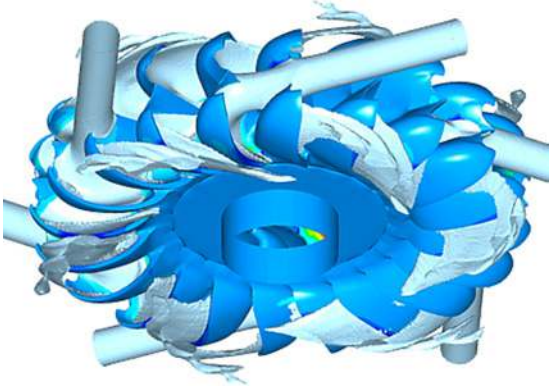|	Length scale D [mm]	Velocity scale C [mm]	Reynolds Re [-]	Froude Fr [-]	Weber We [-]
Confined flow	200	4.5	0.5×10^6	3	-
Water jet	30	40	0.6×10^6	80	15
Bucket flow	300	20	3×10^6	12	40
Water droplet	1	5	0.003×10^6	100	0.03

Figure 3   Jets and water sheets around a Pelton runner simulated with ANSYS-CFX®
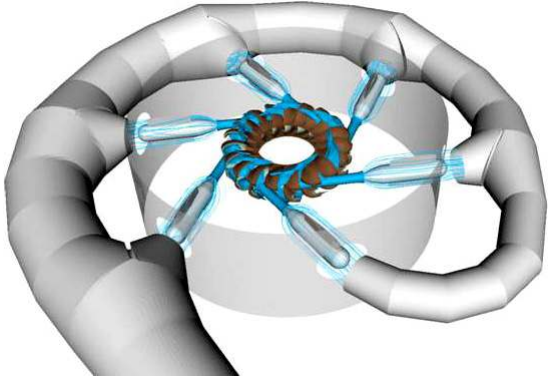

Figure 4   Numerical simulation of a complete Pelton turbine (distributor, runner and casing) with ANSYS-CFX®

approach. By nature, a lagrangian description has better capacities to track interfaces properly. But to take full benefit of the lagrangian feature, a numerical method should rely on a true mesh-less numerical scheme, as it allows any distorsion of the calculation points distribution. The *Smoothed Particle Hydrodynamics* (SPH) method corresponds to this requirement and was first tested in its standard form, as depicted by Monaghan, for example in Monaghan *et al.* (1994). Some limitations were identified, mainly linked to the accuracy and the treatment of boundary conditions (Marongiu *et al.* 2007). This explains why some adaptations were achieved, leading to the development of an hybrid method called the SPH-ALE method.

2   The SPH-ALE method

2.1   *Introduction*

The SPH-ALE method was mainly developed by Vila (1999). It is based on the standard SPH method but differs in the way flow is described. The SPH method is often presented as a whole, but it may be of high value to consider the core of the method (its mesh-less numerical scheme) separately from the other aspects (lagrangian flow description, particle interactions modelling).

2.2   *Principles*

The SPH-ALE adopts a dual description called *Aritrary Lagrange Euler*. It consists in writing the conservation laws, here for an

inviscid flow, in a moving frame of reference, whose velocity v_0 can be chosen arbitrarily. We thus consider the following system of conservation laws written for a control volume Ω moving with speed v_0:

$$\frac{d}{dt}\Big|_{v_0} \int_\Omega \Phi \, d\Omega + \int_S \Phi(v - v_0) \cdot n \, dS$$
$$= \int_S Q_S \cdot n \, dS + \int_\Omega Q_V \, d\Omega \tag{1}$$

Φ is the vector of conservative variables. S is the boundary of Ω, n the unit outward normal vector, Q_S and Q_V the surface and volume source terms, respectively. $\frac{d}{dt}\big|_{v_0}$ stands for a time derivative along the trajectory of the control volume. Considering that the surface source term can be reduced to the pressure term, (1) becomes:

$$L_{\vec{v}_0}(\Phi) + \mathrm{div}(F_E(\Phi) - v_o\Phi) = Q_V \tag{2}$$

where $L_{\vec{v}_o}(\Phi)$ is the transport operator associated with the transport field v_0 and F_E is the flux vector of the Euler equations. In two space dimensions, this can be expressed as:

$$\Phi = \begin{pmatrix} \rho \\ \rho v^{(1)} \\ \rho v^{(2)} \end{pmatrix}, \quad F_E^{(1)}(\Phi) = \begin{pmatrix} \rho v^{(1)} \\ p + \rho(v^{(1)})^2 \\ \rho v^{(1)} v^{(2)} \end{pmatrix},$$
$$F_E^{(2)}(\Phi) = \begin{pmatrix} \rho v^{(2)} \\ \rho v^{(1)} v^{(2)} \\ p + \rho(v^{(2)})^2 \end{pmatrix} \tag{3}$$

The discretization of the weak form (2) by use of SPH spatial derivative operators then leads to the appearance of one-dimensional moving Riemann problems at the interfaces between neighbouring calculation points. Vila (1999) showed that the solution to a moving Riemann problem could be easily linked to the solution of the equivalent steady Riemann problem. It is thus possible to treat interaction between calculation points like numerical fluxes of Godunov type. This feature directly links the SPH-ALE method to the *Finite Volume* (FV) method, and allows a more or less direct adaptation of techniques developed in the field of Eulerian mesh-based methods to SPH-ALE. However it is worth noticing that the use of Godunov numerical fluxes introduces mass fluxes between interacting calculation points, even in the case where the transport field is chosen to be equal to the fluid velocity. Thereby calculation points should no more be considered as particles (as they usually are by SPH practitioners) but as moving control volumes.

The discrete counterpart to the system of conservation laws in (2) is finally expressed by:

$$\frac{d}{dt}(\omega_i \Phi_i) + \omega_i \sum_{j \in D_i} \omega_j 2 G_E(\phi_i, \phi_j) \nabla_i W_{ij} = \omega_i Q_V \tag{4}$$

D_i is the kernel support for particle i and G_E stands for a Godunov flux adapted to the moving Riemann problem.

2.3 Riemann solvers

The system (4) requires the solution of the non linear moving Riemann problems which appear between each pair of neighbouring points. However the exact solution can only be obtained through an iterative and costly procedure. Approximate solutions of various types are usually considered in practical numerical methods, for example by linearizing the original Riemann problem. In the following, the VFRoe scheme and its preconditioned version, the VFRoe-Turkel scheme, are exposed.

2.3.1 VFRoe scheme

The VFRoe scheme, introduced by Gallouet and Masella (1996), solves a linearized Riemann problem between left and right states. It differs from the traditional Roe scheme because the linearized jacobian matrix $\tilde{A}(\Phi_L, \Phi_R) = \frac{\partial F}{\partial \Phi}$ does not have to fulfill the consistency relation known as the Roe condition.

The procedure that leads to the solution is based on a projection of the jump between left and right states onto right eigenvectors of the jacobian matrix. In the end, the solution appears as a combination of a centered contribution and an upwind one, and considering that the equation of state used is the Tait equation, it is given by:

$$
\begin{cases}
\rho^* = \frac{1}{2}(\rho_L + \rho_R) - \frac{1}{2\tilde{c}} - (\rho v_R - \rho v_L) \\
\rho v^* = \frac{1}{2}(\rho v_L + \rho v_R) - \frac{\tilde{c}}{2} - (\rho_R - \rho_L)
\end{cases}
\tag{5}
$$

The upwind contribution helps to stabilize the scheme but it is also responsible for the numerical diffusion. It can be seen that this numerical diffusion is proportional to the jump between left and right states.

2.3.2 VFRoe-Turkel scheme

The VFRoe scheme presented above suffers from excessive numerical diffusion and produces noisy pressure fields. The use of Godunov type schemes in the limit of low Mach numbers as encountered in hydraulic flows is known to lead to this type of results (Guillard and Murrone 2004). Preconditioning of the Riemann solver can be an efficient way to improve this behaviour. Preconditioning techniques were initially developed to speed-up convergence to a steady state (Turkel 1987). This results in a formulation which is not consistent in time. But it was also found that the preconditioning of the numerical diffusion term can greatly reduce numerical oscillations (Viozat 1997). The VFRoe-Turkel scheme is consequently based on the VFRoe scheme, in which the dissipation term is modified by the preconditioner of Turkel. The procedure described above for the VFRoe scheme can thus be applied to a modified (preconditioned) Riemann problem whose jacobian matrix is $\tilde{P}\tilde{A}$ where

$$
\tilde{P} = \begin{bmatrix} \tilde{\beta}^2 & 0 \\ 0 & 1 \end{bmatrix}
\tag{6}
$$

is the preconditioner of Turkel and $\tilde{\beta} \approx \tilde{M}_a$. This preconditioner is initially written for entropic variables but its expression remains unchanged when transformed into conservative variables

when the Tait equation of state is used. Finally the solution to the preconditioned Riemann problem is given by:

$$
\begin{cases}
\rho^* = \frac{1}{2}(\rho_R + \rho_L) \\
\quad - \frac{1}{2}\left[\tilde{v}(\tilde{\beta}^2 - 1)\left(\frac{\rho_R - \rho_L}{\sqrt{\Delta}} + \frac{\tilde{v}(1 - \tilde{\beta}^2)}{2\tilde{c}^2 \sqrt{\Delta}}(\rho v_R - \rho v_L) \right) \right. \\
\quad \left. + \frac{\sqrt{\Delta}}{2\tilde{c}^2}(\rho v_R - \rho v_L) \right] \\
\rho v^* = \frac{1}{2}(\rho v_R + \rho v_L) \\
\quad - \tilde{c}^2\left(\frac{\rho v_R - \rho_L}{\sqrt{\Delta}} + \frac{\tilde{v}(1 - \tilde{\beta}^2)}{2\tilde{c}^2 \sqrt{\Delta}}(\rho v_R - \rho v_L) \right)
\end{cases}
\tag{7}
$$

with $\Delta = \tilde{v}^2(1 + \tilde{\beta}^2)^2 - 4\tilde{\beta}^2(\tilde{v}^2 - \tilde{c}^2)$. It can be verified that when $\tilde{\beta} = 1$, VFRoe-Turkel and VFRoe schemes are equivalent. On the other hand when $\tilde{\beta} \to 0$ then all eigenvalues of the modified jacobian matrix are of the order of $\tilde{v}$ thus greatly reducing the condition number. Near stagnation points, stability of the preconditioned scheme tends to degrade and the value of $\tilde{\beta}$ has to be limited to prevent its fall to zero. Following recommendations by Turkel (1999) we use:

$$
\tilde{\beta}_{ij} = \min(1, \max(k_1 \tilde{M}a, \max(\beta^i_{\min}, \beta^j_{\min}))),
$$

$$
\beta^i_{\min} = \max_{j \in D_i} \left(\frac{p_j - p_i}{\rho_{ij} c_{ij}^2} + \frac{\|v_j - v_i\|}{c_{ij}} \right)
\tag{8}
$$

2.3.3 Second order scheme

The two schemes presented above are only first order accurate in space because they are based on a piecewise constant approximation of the solution. Because the SPH numerical stencil is much wider than those encountered in mesh-based methods, the amount of numerical dissipation is higher and can become prohibitive. Following an approach similar to the MUSCL scheme developed by Van Leer (1979), a second order scheme is introduced by replacing the piecewise constant by a piecewise linear approximation of the solution. Gradients of field variables are so first computed using the SPH method and then used to extrapolate field values from particle centers to interfaces between interacting points by applying the following formulas:

$$
\begin{cases}
\Phi_L = \Phi_i + \xi(\Phi_i, \Phi_j, \nabla_i \Phi) \cdot \frac{(x_j - x_i)}{2} \\
\Phi_R = \Phi_j - \xi(\Phi_j, \Phi_i, \nabla_j \Phi) \cdot \frac{(x_j - x_i)}{2}
\end{cases}
\tag{9}
$$

where ξ is a non-linear function acting as a limiter of gradients slopes. The introduction of these limiters is compulsory to remove the spurious oscillations appearing in sharp gradients zones.

2.4 Boundary conditions

In the ALE framework, the handling of boundary conditions can be much more adequately set than in the standard SPH method.

This is mainly due to the choice of an ALE description, which enables the treatment of a boundary surface travelling with its own velocity, independently of the fluid velocity. It will be shown that upwinding is also of great interest to translate effects of the fluid onto the boundary, and inversely. The proposed boundary treatment can be split into two steps. In the first, a mathematically consistent approximation of the boundary term is deduced from the kernel approximation itself. Its discrete counterpart, similar to a particle approximation, leads to the setup of boundary fluxes. These boundary fluxes are, in the second step, computed in an upwind fashion, after an interpretation of the mutual influence of the fluid and the boundary condition as a partial Riemann problem.

2.4.1 *Surface integral boundary term*

Most of the existing boundary treatments are facing the difficult task to add extra calculation points outside the computation domain. This is mandatory so as to cope with truncated kernel supports in the vicinity of a boundary. In practice the spatial distribution of these points is not easy to set because of geometric issues and field values attributed to these points can be obtained only through a long-range (the size of the kernel support) extrapolation of the field from inside the fluid domain. Besides, in order to be accurate, this extrapolation should be non-linear (as Euler equations).

The standard way to obtain the SPH approximation of gradients starts from an integration by parts given by:

$$\langle \nabla f(x) \rangle = \int_{\partial D(x)} f(x') W(x - x') n dS$$
$$- \int_{D(x)} f(x') \nabla_{x'} W(x - x') \, dV \qquad (10)$$

where $\partial D(x)$ is the intersection of the kernel support with the boundary. The surface integral term is usually neglected because of the use of compactly supported kernel functions. Most of the available boundary treatments try to compensate for this term with a volume term.

It is proposed here to compute this term directly, as a surface term. Doing so, the previous difficulties can be avoided. In pratice, the particle approximation of this surface term is obtained using the same quadrature formula as the one used for the volume term, provided a satisfactory discretization of the boundary surface is available. In term of fluxes budget, boundary fluxes are

finally expressed as:

$$\int_{\partial D_i} (F_E(\Phi) - v_0 \Phi) W(x_i - x') n dS$$
$$= \sum_{j \in \partial D_i} \omega_j G_E(\Phi_i, \Phi_j) W_{ij} n_j \qquad (11)$$

ω_j is the weight of the boundary element j (area of the surface element in 3D) which samples the boundary and n_j is the unit normal vector to the boundary at location x_j. $G_E(\Phi_i, \Phi_j)$ is a boundary Godunov flux which is explicited in the next step.

2.4.2 *Partial Riemann problem*

The Riemann problem described previously is used to determine the mutual influence of two fluid states, namely the left state and the right state. Considering now the interaction of a fluid state, let's say a left state, and a boundary condition, it is clear that no right state can be defined. However, the influence of the boundary on the numerical solution is computed through boundary fluxes arising at the boundary surface. The boundary surface thus plays a similar role as the one played by an interface between two fluid states. Following Dubois (2001), the boundary surface can hence be taken for an interface of a partial Riemann problem, for which one state is missing. Nevertheless, the solution to this partial Riemann problem is partially defined by the physical boundary conditions imposed on the boundary surface. The whole solution consequently results from the selection, among all the states compatible with the imposed boundary condition, of the one which can be reached from the left state through a shock or a rarefaction wave. Figure 5 helps understanding this concept.

We consider a one dimensional partial Riemann problem along the normal direction to the boundary, between a given left (fluid) state Φ_L and a boundary surface. Primitive variables are noted ρ and v where v stands for the normal component of the velocity field. The imposed boundary condition turns out to be a given relation (implicit or explicit) between ρ and v and is stated in a general form $B(\rho, v) = 0$. If two conditions are imposed, the solution is fully determined by the boundary condition and the fluid state plays no role. This configuration corresponds to a supersonic inlet for instance. On the contrary, if no boundary condition is imposed, the solution is fully determined by the fluid state, it's the case of a supersonic outlet. The general case where only one condition is imposed is now considered. In the $\rho - v$ diagram, the relation $B(\rho, v) = 0$ can be represented by a
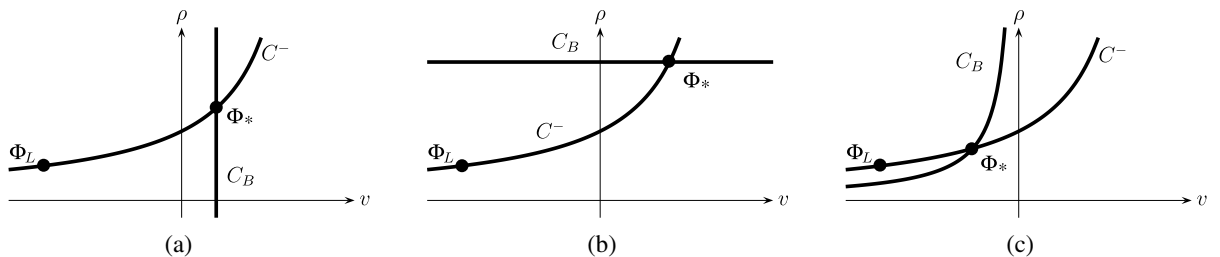
Figure 5 Different configurations corresponding to usual boundary conditions. (a) Case of a solid wall or a subsonic inlet: velocity imposed; (b) Case of a subsonic outlet: pressure imposed; (c) Case of a subsonic inlet: discharge imposed

continuous curve noted C^B. This curve describes the set of states that are compatible with the boundary condition. We can also define the curve, noted C^-, which describes the set of states that can be reached from the left state through either a shock or a rarefaction wave. The solution Φ to the partial Riemann problem is finally the intersection point between these two curves. Some usual configurations are given in Fig. 5.

It is worth noticing that this boundary modelling can be used for any kind of boundary condition, and that it naturally treats boundaries in the same way as the interior scheme treats fluid interactions.

3 Application to Pelton turbines

3.1 *Introduction*

The SPH-ALE method presented is used to simulate free surface flows in Pelton buckets, in a static and a rotating configuration. Numerical simulations are done at model scale, which is a usual setup for mesh-based simulations. In order to save some computational cost, a symmetry condition is used.

3.2 *Symmetry condition*

The main components of a Pelton turbine are usually symmetric against the middle plane of the runner. It is obviously the case for the runner, and at first sight for the distributor and the injectors. The upstream parts, like the penstock and the intermediate bifurcations, present however some bends which are responsible for secondary flows in the jets. Nevertheless the way jets are discretized at the moment does not allow to take account of these secondary flows, and jets involved in the following simulations have a flat velocity profile at the inlet condition. The casing is a component which is not symmetric in general, but the present study is restricted to flows in the immediate neighbourhood of the buckets and so the casing is not incorporated in simulations. It is thus possible to consider the flows we are interested in as symmetric, and to divide the computational domain size by a factor two. But for the correctness of simulations, the removed part must be replaced by a symmetry condition. This is obtained by adding fictitious fluxes in the flux balance of particles whose kernel support intersects the symmetry plane. These fictitious fluxes are computed in a way similar to the well-known technique of ghost particles (Colagrossi and Landrini 2003).

3.3 *Free surface flow in a steady Pelton bucket*

The first application considered is a steady Pelton bucket impinged by a water jet. The jet velocity is $C = 19.61$ m/s and its diameter is $d_0 = 3$ cm. The discretization size is $\Delta x = 1$ mm. The simulation represents a physical time of approximately 22 ms, so as to obtain a converged state in time. The number of particles involved is 93000 at the end of the simulation. Only the inner surface of the bucket is considered, its discretization uses a surface triangulation achieved with the commercial mesh tool ICEM®. This triangulation is refined near sharp geometrical

details like the leading edge. The bucket is thus represented by a set of 48738 surface elements.

The artificial speed of sound used in the Tait equation of state is set to $c_0 = 200$ m/s, and the reference density of water is $\rho_0 = 1000$ kg/m³. Figure 6 shows a view of the case. It can be seen that the escaping water sheet can be properly represented far from the trailing edge of the bucket, showing that the lagrangian description allows a proper tracking of interfaces on long distances.

Pressure distribution on the bucket surface is closely examined (see Fig. 7). Results are compared with measurements and CFX® results at some given locations corresponding to pressure sensors locations (see Fig. 8). Figure 9 shows the pressure profiles along two lines of sensors. The hybrid method tends to underestimate the value of the pressure coefficient. Results are here presented using one sensor as the reference, which enables to compare the evolution only.

The influence of the use of the preconditioned scheme is studied through two aspects: the noise of the pressure field and the thickness of the water sheet in the bucket. Figure 10 shows on the
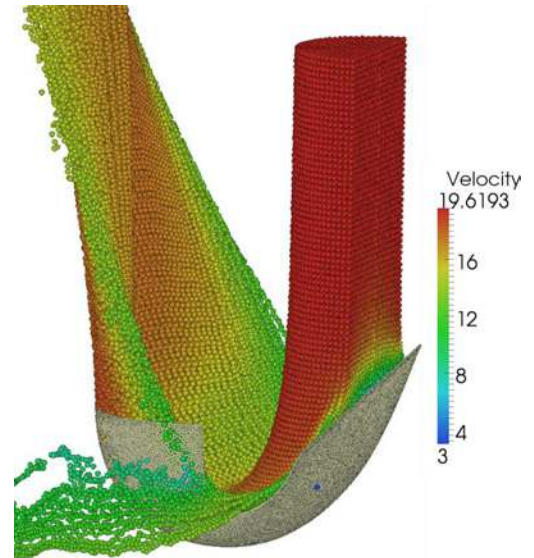

Figure 6 General view of the case. Fluid particles coloured by their velocity
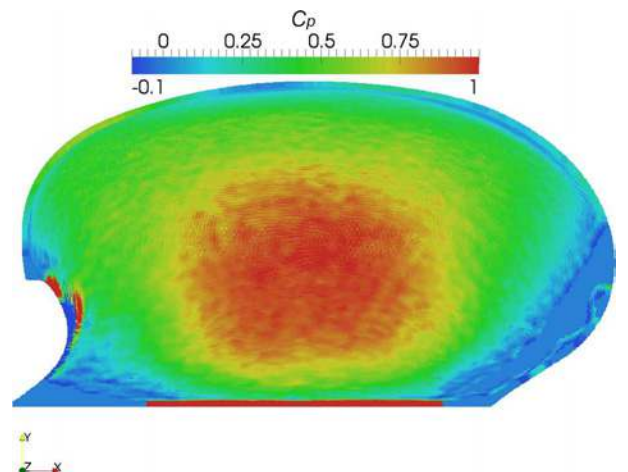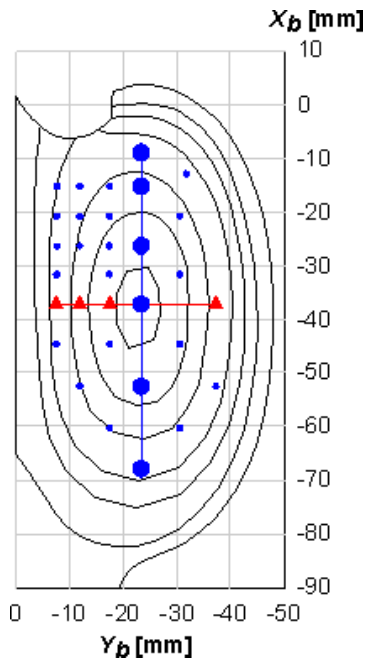

Figure 7 Pressure coefficient map on the bucket surface

6

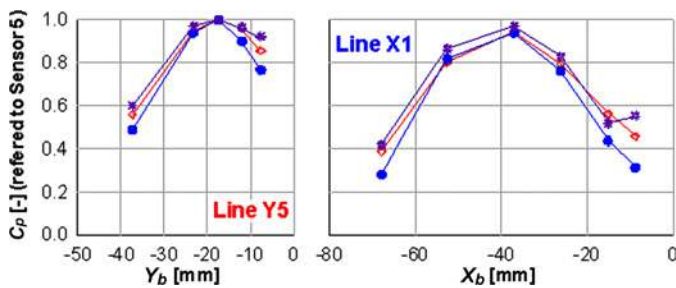Figure 8   Position of the pressure sensors and mark of the plotted lines

top left that the VFRoe-Turkel scheme produces a slightly thiner water sheet than the VFRoe scheme. The benefit of the preconditioned scheme is also visible in the same figure on the top right and bottom, where particle data have been interpolated on a regular cartesian grid for visualization. Both schemes produce a high pressure zone at the leading edge (region noted 2). This comes from the geometrical representation of the leading edge, with a small flat surface instead of a purely sharp edge. It can be seen that the CFX simulation produces the same stagnation point, but the fact that the mesh is finer in this region (to catch the boundary layer) tends to reduce its influence. On the contrary, because a constant discretization size is used in SPH-ALE simulations, this phenomenon is strong enough to generate a small detachment bubble downstream (low pressure zone). In other regions of the flow (noted 1, 3 and 4), the shapes of the isolines obtained with the VFRoe-Turkel scheme are smoother than those obtained with the VFRoe scheme, and are also closer to those obtained with CFX. It has to be noticed that the SPH-ALE results presented are instantaneous results. A time averaging procedure would have smoothed the results but also hidden differences between both schemes.

Figure 9   Pressure profiles along the X1 and Y5 lines. Pink stars: experiments. Red diamonds: CFX®. Blue dots: SPH-ALE method

3.4   *Free surface flow in a rotating bucket*

The flow in a single rotating Pelton bucket is then studied. The discretization size is once again 1 mm, jet velocity is $C = 33.6145$ m/s, which corresponds to a water head of 60 m, jet diameter is 22 mm and rotation speed of the bucket is 95.4908 rad/s. This time, it is necessary to use not only the inner surface of the bucket, but the whole bucket, which represents 91596 surface elements. The simulation represents a physical time of 8.4 ms during which the bucket makes a rotation of 46°.
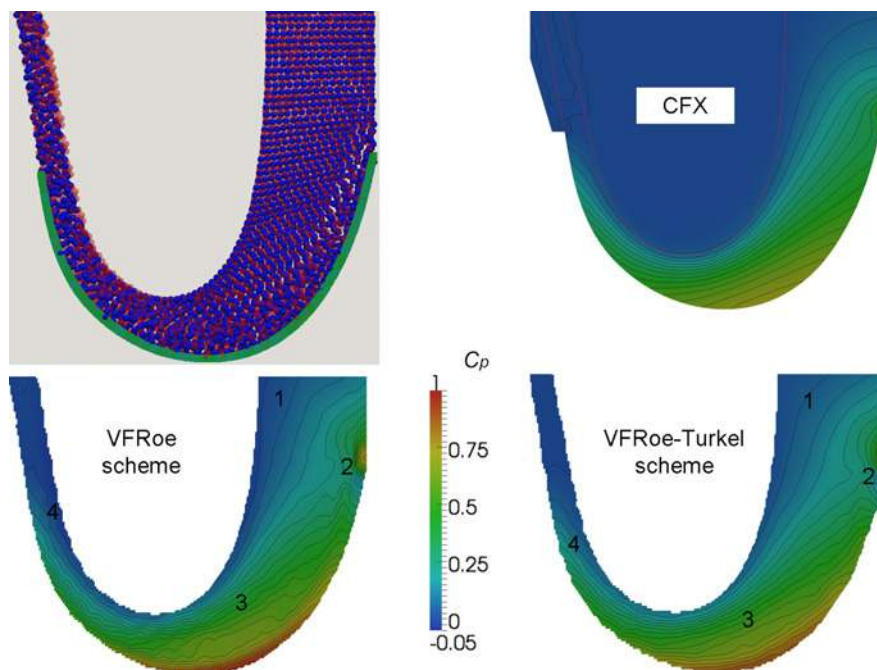

Figure 10   Comparison of numerical results obtained with the VFRoe and the VFRoe-Turkel schemes, and CFX. Top left: water sheets thicknesses. Light red spheres: VFRoe scheme. Blue spheres: VFRoe-Turkel scheme. Top right and bottom: pressure coefficient field and isolines of pressure coefficient with both schemes (particle data interpolated on a regular grid). Red line: isoline 0.5 of volume fraction obtained with CFX (position of the free surface)

(a) T = 3.2 ms.

(b) T = 3.2 ms.

(c) T = 6 ms.

(d) T = 6 ms.

(e) T = 8.4 ms.

(f) T = 8.4 ms.

Velocity

10.0   20.0   30.0
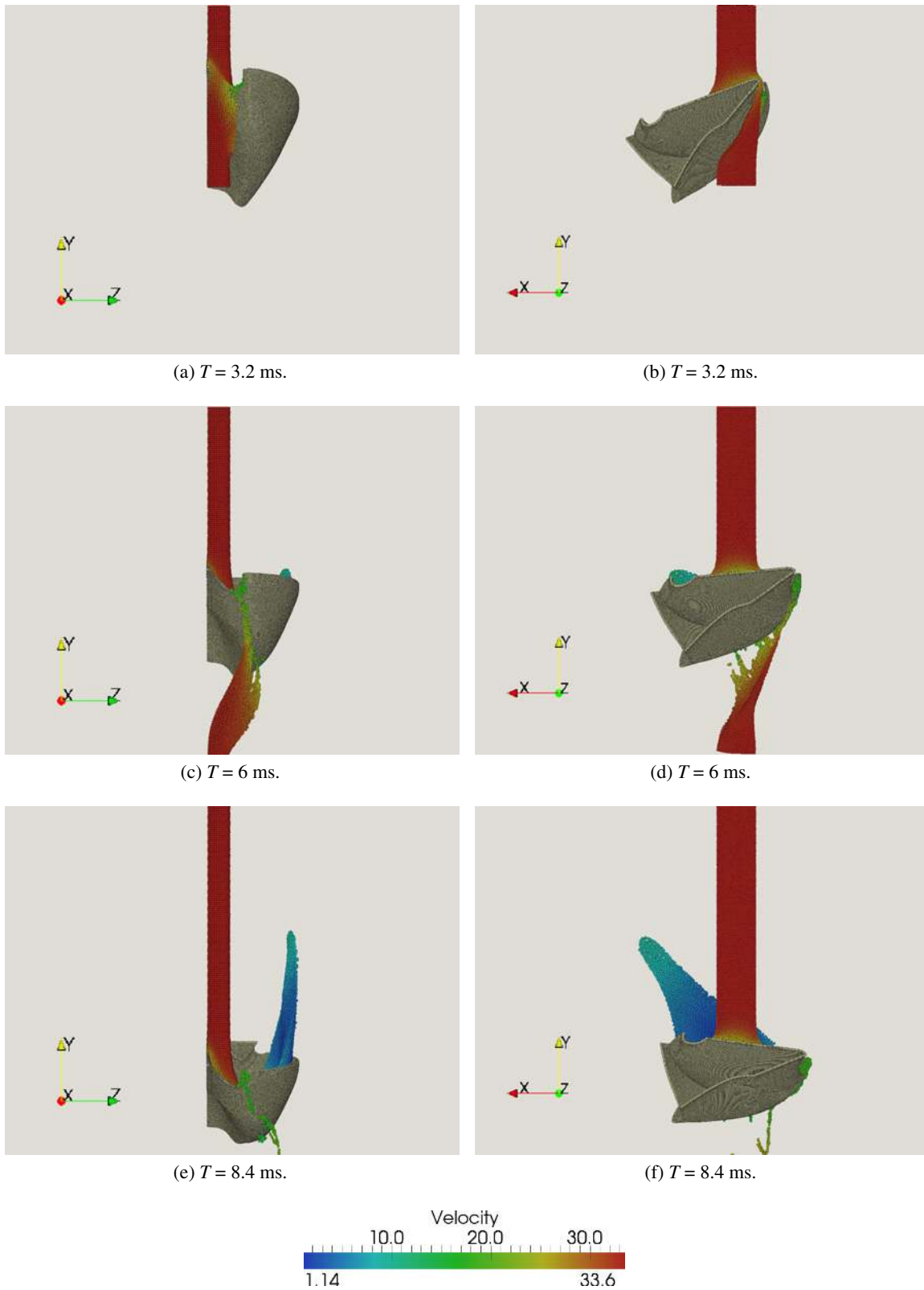
1.14   33.6

Figure 11   Views of the rotating bucket case at different times, along X axis (left) and Z axis (right). Fluid particles are coloured by their velocity

Figure 11 present some views of this simulation at different times. The behaviour of the flow is satisfactory. For instance it can be seen that the escaping water sheet has a residual velocity which is very small in the absolute frame of reference, which is the result of the exchange of energy between the jet and the bucket during the rotation. This is also shown on Fig. 12, where the evolution of the hydraulic torque during the rotation is plotted for both the SPH-ALE method and CFX®. For the SPH-ALE method, the torque is obtained by integrating the torque contributions coming from the pressure field on the bucket surface. For CFX, viscous contributions are also taken into account. In Fig. 12, torque values have been divided by the maximum values, so that it is possible to compare the evolution during the rotation. It can be seen that some differences between the two curves exist at the beginning
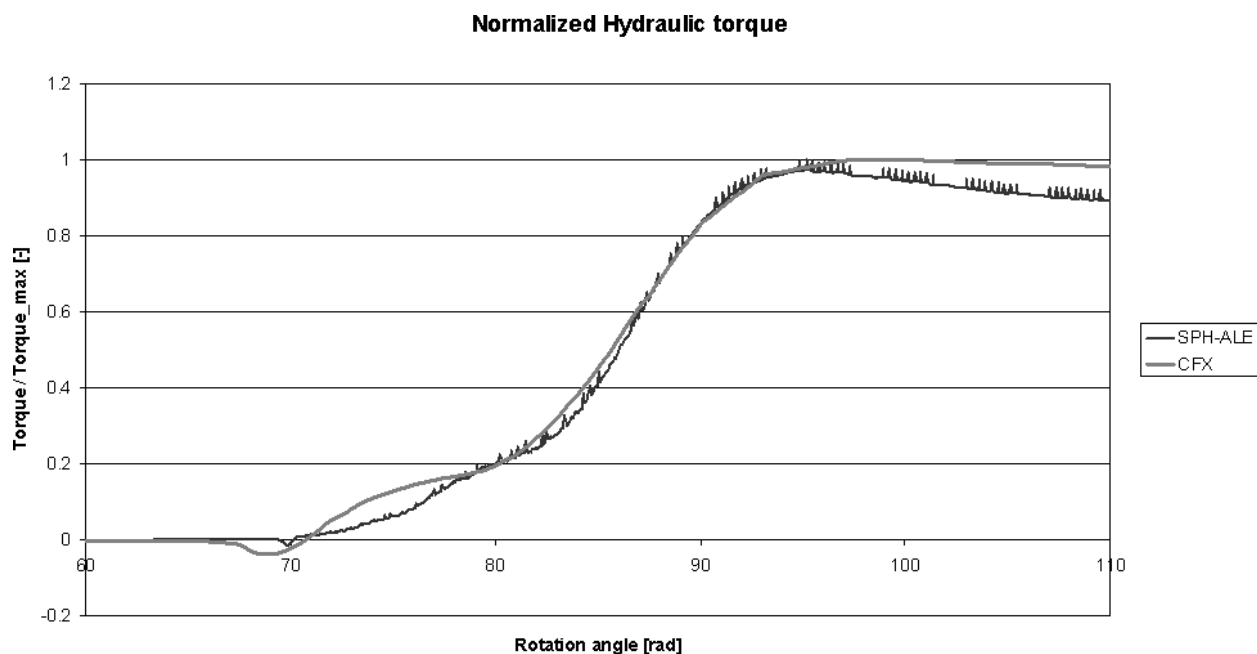
Normalized Hydraulic torque

Figure 12   Hydraulic torque predicted by the SPH-ALE method and CFX

of the jet-bucket interaction and also after the peak (these latter are due to a slightly different geometry of the bucket root). But the agreement between the two curves is globally good.

4   Conclusion

It has been shown that a shift of the flow description commonly used in the SPH method can help overcoming some of the major weaknesses that restrict the use of this numerical technique. The ALE description, together with the use of a conservative form of the Euler equations, enables to link the SPH method to more traditional numerical methods like the finite volumes method, taking the best of each. It is then possible to adapt the large amount of models developed for these methods to set a kind of hybrid method. In particular, it is shown in this paper that the use of Godunov schemes greatly increases the stability and produces pressure fields with much less numerical noise. Accuracy can be improved through the introduction of higher order schemes and preconditioning techniques. A general technique to treat boundary conditions is also presented. It takes full benefit from the upwinding used in the interior scheme to extrapolate the field to the boundary while respecting the imposed physical boundary condition. The boundary influence is added as a boundary flux in the conservation laws. As only the discretization of the boundary surface is required, this technique is able to treat boundary conditions of any shape. Even if some flow details are not accurately captured yet, the SPH-ALE method can be already used to simulate realistic complex free surface flows. This opens the door to simulate flows in Pelton turbines. It is expected that the connexion between this SPH-ALE method and the finite volume framework will ease the widening of the modeling skills of the SPH-ALE. For example viscous effects should be included to take into account their contribution to the hydraulic torque. Nevertheless, the accuracy of the method is still dependent from the relatively simple SPH integration scheme. A great challenge resides in finding a more accurate mesh-less numerical scheme that could compete with high-order mesh-based schemes.

Notation

c = Local speed of sound

c_0 = Reference speed of sound

C_p = Pressure coefficient ($= p/\rho g H$ or equivalently $= p/(0.5\rho C_{\text{jet}}^2)$)

D = Interpolation domain

h = Smoothing length

i = Particle index

n = Normal vector to the boundary

Φ = Vector of conservative variables

v = Fluid velocity field

v_0 = Transport velocity field

W = Kernel function

x = Position

p = Density

w = Particle volume (weight)

Ω = Fluid domain

β = Preconditioning parameter

Subscripts and symbols

$\tilde{} =$ Averaged variable at a linearized intermediate state
$* =$ Solution to a Riemann problem
$L =$ Value on the left side of a Riemann problem
$R =$ value on the right side of a Riemann problem

References

Colagrossi, A., Landrini, M. (2003). Numerical simulation of interfacial flows by Smoothed Particle Hydrodynamics. *J. Comput. Phys.* 191, 448–475.

Dubois, F. (2001). Partial Riemann problem, boundary conditions, and gas dynamics. *Absorbing boundaries and layers, domain decomposition methods: Applications to large scale computations*, 16–77. Nova Science Publishers Inc.

Favre, J.M., Garcin, H., Parkinson, E. (2005). Computational analysis in Pelton hydraulic turbines. 23rd *CADFEM users' meeting*, Bonn, Germany.

Gallouet, T., Masella, J.M. (1996). A rough Godunov scheme. *C. R. Academy of Science Paris* I-323, 77–84.

Guillard, H., Murrone, A. (2004). On the behaviour of upwind schemes in the low Mach number limit II: Godunov type schemes. *Compuiters and Fluids* 33, 655–675.

Kvicinsky, S., Kueny, J.L., Avellan, F., Parkinson, E. (2002). Experimental and numerical analysis of free surface flows in a rotating bucket. Proc. 21st *IAHR symposium on hydraulic machinery and systems*, 483–490, Lausanne, Switzerland.

Marongiu, J.C., Leboeuf, F., Parkinson, E. (2007). Numerical simulation of the flow in a Pelton turbine using the meshless method smoothed particle hydrodynamics: a new simple solid boundary treatment. Proc. *IMechE, Part A: J. Power and Energy* 221, 849–856.

Monaghan, J.J., Thompson, M.C., Hourigan, K. (1994). Simulation of free surface flows with SPH. Proc. *ASME symposium on computational methods in fluid dynamics*, Lake Tahoe, USA.

Parkinson, E., Geppert, L., Chapuis, L., Vullioud, G. (2004). Major rehabilitation of the Pelton units of The Bridge River and Kemano power plants. *Hydrovision*, Montreal, Canada.

Perrig, A. (2007). Hydrodynamics of the free surface flow in Pelton turbine buckets. *PhD thesis*. École Polytechnique Fédérale de Lausanne.

Perrig, A., Avellan, F., Kueny, J.L., Fahrat, M., Parkinson, E. (2006), Flow in a Pelton turbine bucket: numerical and experimental investigations. *J. Fluids Engng.* 128, 350–358.

Turkel, E. (1987). Preconditioned methods for solving the incompressible and low speed compressible equations. *J. Comput. Phys.* 72, 277–298.

Turkel, E. (1999). Preconditioning techniques in computational fluid dynamics. *Annual Rev. Fluid Mech.* 31, 385–416.

Van Leer, B. (1979). Towards the ultimate conservative difference scheme V: a second order sequel to Godunov's method. *J. Comput. Phys.* 32, 101–136.

Vila, J.P (1999). On particle weighted methods and Smoothed Particle Hydrodynamics. *Math. Mod. Meth. Appl. Sci.* 9, 161–209.

Viozat, C. (1997). Implicit upwind schemes for low mach number compressible flows. *Technical report, INRIA*.